Build Simul (2018) 11: 677–694
https://doi.org/10.1007/s12273-018-0434-z

Numerical study on cooling performance of a ventilated Trombe wall with phase change materials

Xiaohong Liu[1,3,5], Yuekuan Zhou[2,3,4] (✉), Guoqiang Zhang[1,2,3]

1. *College of Architecture, Hunan University, Changsha, Hunan 410082, China*
2. *College of Civil Engineering, Hunan University, Changsha, Hunan 410082, China*
3. *National Center for International Research Collaboration in Building Safety and Environment, Hunan University, Changsha, Hunan 410082, China*
4. *Department of Building Services Engineering, Faculty of Construction and Environment, The Hong Kong Polytechnic University, Hong Kong, China*
5. *Hunan University Design Institute Co., LTD, Changsha , Hunan 410082, China*

Abstract

This study aims to evaluate thermal performance of a new ventilated Trombe wall integrated with phase change materials (PCMs-VTW). Double PCM wallboards are embedded in the building facade for different purposes, i.e. exterior PCM wallboard is to store natural cooling energy via night-time ventilation, and interior active PCM wallboard is for radiant cooling. Melting temperature and latent heat of PCM have been discussed for PCMs-VTW system from 1st August to 7th August in Changsha, China. Also, high-reflective coating is coated on the exterior PCM wallboard for reflecting solar radiation, thus ameliorating daytime overheating. Nighttime ventilation is for natural cooling energy storage via regenerating solid exterior PCM wallboard. The obtained result shows that under the weather condition in Changsha, melting temperature 22 °C for interior PCM and the latent heat 176 kJ/kg for exterior PCM show considerable benefit for cooling energy release. Compared with the classical Trombe wall system, annual cooling energy consumption is decreased by 20.8% and by 18.6% in the PCMs-VTW system when indoor air temperature is kept at 22 °C and 24 °C respectively. Our research has provided scientific evidences for potentials provided by PCMs-VTW system in reducing building energy consumption and improving indoor thermal comfort via exploiting natural cooling energy, mitigating overheating at summer condition and utilizing cold sources in high temperature.

Keywords

phase change material,
Trombe wall,
ventilation,
cooling energy storage,
high-reflective coating

Article History

Received: 2 August 2017
Revised: 16 January 2018
Accepted: 22 January 2018

1 Introduction

With the rapid growth in population as well as the improved requirement in indoor environment, building energy consumption including heating, ventilation and air conditioning (HVAC) has been drastically increasing, which matches against the limited quantity in total amount of non-renewable energy. Renewable energy utilization technologies are highly desirable to be developed to reduce the dependence on non-renewable energy due to its environmental-friendliness and sustainability (Sharma et al. 2009). But the main hindrance for its popularization is due to its uneven spatial distribution, intermittence in temporal distribution, instability, and stochastic characteristic (Cao and Sirén 2014, 2015; Feng et al. 2016). To overcome these problems, latent heat storage system with phase change material (PCM) has been widely used due to its high heat storage capacity, small volume change on phase transformation, non-corrosiveness and nontoxicity (Mavrigiannaki and Ampatzi 2016; Bourne and Novoselac 2015; Nikoofard et al. 2015; Zhou et al. 2017). PCM Trombe wall is one of the feasible and sustainable technologies for efficiently utilizing solar energy in HVAC system. It is generally composed by a massive wall integrated with PCM, an exterior glazing cover and a ventilated air gap between the wall and the glazing (Soares et al. 2017; Fiorito 2012; Saadatian et al. 2012). Solar radiation transmitting through the glazing is stored by PCM wall. After being embedded with PCM Trombe wall system, building energy

E-mail: yk.zhou@polyu.edu.hk

List of symbols

C	specific heat capacity [kJ/(kg·°C)]
D	width of the channel [m]
F	area [m^2]
g	gravitational acceleration [m/s^2]
h	coefficient of heat transfer [W/(m^2·°C)]
h_{w1}	convective heat transfer coefficient of internal surface under natural ventilation [W/(m^2·K)]
h_{f2}	convective heat transfer coefficient for interior PCM wallboard [W/(m^2·°C)]
H	latent heat of PCM [kJ/kg]
I	solar radiation [W/m^2]
L	width of the room [m]
L_1	thicknesses of exterior PCM wallboard [m]
L_2	medium structure [m]
L_3	interior active PCM wallboard [m]
m	mass flow rate [kg/s]
n	air change rate [h^{-1}]
Nu	Nusslet number
P	height of the room [m]
Pr	Prandtl number
ΔP	pressure difference [Pa]
q	heat flux [W/m^2]
Q	annual cooling energy consumption [kWh]
Q_{lw}	long wave radiation [W/m^2]
r	number of the node
R	heat convective resistance [m^2·°C /W]
Re	Reynolds number
Ra	Rayleigh number
s	PCM phase transitioning position [m]
T	temperature [°C]
t	time [s]
u	airflow rate [m/s]
W	length of the channel [m]
X	angle factor
X_{21}	angle factor among floor to wall
x	solid–liquid interface of PCM wallboard
α	absorbance; thermal diffusivity coefficient [m^2/s]
β	volume expansion coefficient of air [°C^{-1}]
ε	emittance
λ	thermal conductivity [W/(m·°C)]
ν	kinematic viscosity of air [m^2/s]
ξ	resistance coefficient
ρ	density [kg/m^3]
σ	Stefan-Boltzmann constant [W/(m^2·°C ^{4})]
τ	time step [s]; transmittance

Subscripts

a,f,out	air flowing through the channel
a,in	indoor air
a	air
eq	equal
end	end of the simulation period
Exp	experiment
f	floor
f, wout	outdoor air
f2	interior PCM wallboard
g	ground;
i	node i
in	indoor air
l	liquid
lenshui	cold water
m,i	melting temperature of interior PCM
out	outdoor
os	surfaces of the room
pcm,l	liquid PCM
ret	return
s	solid
shyl	liquid hydrated salt
shys	solid hydrated salt
shy	PCM, inorganic hydrated salt
sky	sky
sup	supply
Sim	Simulation
1	node 1, glazing layer
3	node 3, coating layer
12	node 12, interior active PCM wallboard

Abbreviations

RE	relative error
RMSE	root mean square error
PCMs-VTW	ventilated Trombe wall integrated with phase change materials

consumption would be reduced by 30% (Borreguero et al. 2011) without sacrificing indoor thermal comfort.

Previous studies mainly focused on Trombe wall for passive solar heating in different climate regions all over the world. In subtropical desert climate, Baghdad, Iraq, Khalifa et al. (2009) developed a numerical model to compare indoor thermal performance of rooms fabricated with three different storage materials: concrete, hydrated salt $CaCl_2{\cdot}6H_2O$ and paraffin wax (N-eicosane). The result showed that indoor air temperature fluctuated between 18 °C and 22 °C for the wall made from hydrated salt $CaCl_2{\cdot}6H_2O$ while between 15 °C and 25 °C for the other two types. Rabani et al. (2015a) experimentally investigated thermal performance of a Trombe wall with a new design at winter time for Yazd

city (Iran) desert climate. They concluded that the maximum absorber temperature was increased by 10 °C and difference among maximum and minimum temperature of room was decreased as well. In heating dominated region, Hernández-López et al. (2016) evaluated the energy storage performance of Trombe wall in two heating dominated cities of Mexico. The maximum value of energy storage by Trombe wall was 109 MJ in the heating period and 70 MJ during the cooling period. Zhou and Pang (2015a) experimentally studied thermal performance of PCM Trombe wall enhanced by delta winglet vortex generators (DWVG). Heat exchange, heating rate to the indoor air and outlet temperature of the PCM Trombe wall significantly increased with the application of DWVG. Chen et al. (2006) evaluated thermal performance of Trombe wall with the application of shading devices in heating dominated area, Dalian, China. By adopting shading devices, external surface temperature of the Trombe wall would be increased a lot, resulting in significant decrease in convective heat loss when circulating indoor air through the air channel. In Mediterranean climate area, Bellos et al. (2016) designed an innovative Trombe wall with an extra window. In comparison with conventional Trombe wall and the traditional insulated wall, warmer indoor profile could be ensured especially during the hours between noon and afternoon. After conducting a series of experiments in an artificial experimental set-up, Zhou and Pang (2015b) concluded that indoor thermal comfort could be kept for a long time by using PCM in collector–storage wall system for thermal energy storage.

In different climate regions all over the world, there are several studies focusing on the Trombe wall for passive cooling. In Mediterranean climate region, de Gracia et al. (2013) numerically studied the thermal performance of a ventilated facade integrated with PCM for passive cooling. Cooling energy achieved its peak value during mild season while PCMs had difficulties in solidifying completely to store cooling energy during severe summer period unless mass flow rate of air was increased. Hu et al. (2016) numerically analyzed the effect of three parameters (the bind tilt angle, air gap width and wall material together with its thickness) on cooling performance of a ventilated Trombe wall. It indicated that high blind tilt angle and low density material in the wall exerted significant effect on reducing cooling load, which decreased little by increasing the air gap instead. Ghrab-Morcos et al. (1993) pointed out that in hot summer climate area, overhangs could effectively mitigate overheating of exterior wall at midday, and high thermal capacity of the wall contributed directly to stable indoor air temperature coupled with nighttime ventilation. In subtropical desert climate area, Rabani et al. (2015b) experimentally evaluated cooling performance of a new designed Trombe wall in combination with solar chimney and water spraying system. They concluded that during non-sunny periods, previous thermal energy accumulated in Trombe wall significantly contributed to air ventilation. Krüger et al. (2013) have studied both cooling and heating effect of Trombe wall via constructing two test cells (the experimental one equipped with Trombe wall, the reference one without it) in a subtropical location. They indicated that in comparison with the reference test cell, higher performance of the Trombe wall system could be gained in the cold conditions while improvement in cooling effect was limited. Gan (1998) carried out parametrical study of Trombe walls for cooling via computational fluid dynamics (CFD) technique, and revealed that one commendable way to improve the ventilation rate through the air channel was to insulate the interior surface of a Trombe wall.

As for evaluating the contribution of reflective coating to reducing building energy consumption, Hernández-Pérez et al. (2018) experimentally studied thermal performance of concrete roofs with different coatings. They concluded that the reflective white roof generated the lowest value in daily heat gain, between 55% and 78% lower than the gray roof. Joudi et al. (2013) investigated thermal performance of a cabin with reflective coatings on both interior and exterior claddings under different weather conditions. They concluded that reflective coatings for the interior contributed to net heating savings, and reflective coatings on the exterior contributed to net cooling savings. Xamán et al. (2017) demonstrated the advantage in using the combination of insulating material and reflective coating on roof in heating dominated area, Mexico. They indicated that thermal load could be decreased by 32.4% with respect to the traditional roof. In order to mitigate heat island and reduce building thermal loads, Yuan et al. (2015) demonstrated the considerable effectiveness of retro-reflective materials (RRM) compared to other materials with diffuse or mirror reflective characteristics. Shen et al. (2011) comprehensively evaluated the reduction in exterior and interior surface temperatures, globe temperature, mean radiant temperature, and annual electricity consumption by adopting reflective coating via experimental study. However, increase in heating demand will lead to negative all-year effect in Shanghai.

With regard to radiant cooling wall, Romaní et al. (2016, 2018a) pointed out that thermally activated building systems (TABS) made it possible for integrating renewable energy like free-cooling with ground heat exchangers (GHE). More specifically, the radiant cooling wall without internal gains turned out to actualize significant energy savings, while more energy than air-to-air heat pumps was required under domestic and office scheduled internal gains. Despite this, cooling cost was still reduced due to peak load shifting. Moreover, they also developed a transient 2D numerical model for defining optimal ranges for pipes depth and spacing

(Romaní et al. 2018b). Le Dréau et al. (2015) concluded that radiant cooling wall is more efficient than active chilled beam mainly due to the increased ventilation losses. However, cooling load was highly dependent on internal gains. Meggers et al. (2017) adopted radiant cooling and indirect evaporation for "air conditioning", they found that although air temperature was not changed, there was a cooling sensation in the experimental building. Mikeska et al. (2017) conducted that wall radiant cooling system was able to provide cooling power at 29 W/m^2 and 59 W/m^2 of floor area with cooling water temperatures between 21.5 °C and 18.5 °C, resulting in room air temperatures between 25 °C and 22 °C.

However, there are still many problems when the Trombe wall is used in hot climate condition, such as overheating during the daytime and low natural cooling energy storage efficiency at night (Ghrab-Morcos et al. 1993). Moreover, in hot summer and cold winter regions in China, air conditioning systems are usually equipped without supplying fresh air in office buildings. Sick building syndromes (SBS) have arisen with the rising time for people staying in the room due to poor ventilation in office buildings (ASHRAE 2007). Therefore, well-designed ventilated systems are highly desirable to provide healthy and comfortable indoor environment for occupants. To the best of our knowledge, ventilated Trombe wall integrated with PCMs (PCMs-VTW) has the potential to address this issue as fresh air could be introduced into indoor environment. Meanwhile, overheating could be mitigated via high-reflective coating coupled with natural ventilation. Moreover, cooling storage efficiency would, to some extent, be improved by adopting exterior PCM wallboard coupled with mechanical ventilation at nighttime. Also, based on our previous research (Zhou et al. 2016), both annual cooling energy consumption and indoor air relative temperature fluctuation rate could be reduced by 4.53% and 56.2% via being fabricated with active radiant cooling system. The radiant cooling wall has also been validated in terms of reducing local thermal discomfort with reduced vertical air temperature difference (Le Dréau et al. 2015; Meggers et al. 2017; Mikeska et al. 2017). To the author's knowledge, no paper specifically related to the construction and operation of double PCM wallboards for overheating mitigation, natural cooling energy storage efficiency improvement, and energy saving of radiant cooling wall has been published in the scientific literature. Moreover, the investigation of the combination effect of high-reflective coating, PCM wallboard, and ventilation with intelligent operational control on thermal performance improvement is also rare in the scientific literature. The present research aims to comprehensively investigate overall thermal performances, i.e. overheating mitigation, cooling energy storage efficiency improvement, energy saving and extension of indoor thermal comfort period, of a ventilated Trombe wall integrated with PCMs with a new design, and present a numerical method for giving an insight into what extent thermal and energy performances could be improved by this system. The innovation of our research exists as follows:

(1) Radiant cooling makes it possible for exploiting free-cooling via integrating renewable energy like free-cooling with ground heat exchangers (GHE). Meanwhile, interior PCM wallboard could decrease cooling cost via peak load shifting to cover internal gains that free-cooling is unable to cover.
(2) Double PCM wallboards are fabricated with the system for different purposes, i.e. the exterior PCM wallboard is for improvement in natural cooling energy storage efficiency, and the interior one is for radiant cooling.
(3) High-reflective coating as well as natural ventilation is adopted to ameliorate overheating at daytime. Mechanical ventilation is utilized for storing natural cooling energy via regenerating solid exterior PCM wallboard at night.
(4) Fresh air could be introduced into indoor environment for ensuring indoor air quality.

2 System description

2.1 Detailed construction

The detailed construction of the PCMs-VTW system is shown in Fig. 1. PCMs-VTW system is composed by glazing cover, air channel, exterior PCM wallboard, EPS insulation layer, brick and interior active PCM wallboard fitted with cooling water pipes. PCM is encapsulated by closed stainless steel containers, which could be made easily by the developed moulds. Air gap appears when two containers are combined together so cooling water pipes could easily go through the gap. Two rooms are fabricated as the simulation platform, one is the PCMs-VTW system room and the other is the reference room. The configuration of the both rooms is identical except for the PCMs-VTW system.

Khalifa and Abbas (2009) concluded that the indoor air temperature fluctuated between 18 °C and 22 °C in the room made by hydrated salt $CaCl_2{\cdot}6H_2O$ while between 15 °C and 25 °C in the room made by paraffin and concrete. Moreover, electric wires installed inside the wall might lead to fire catastrophe. Paraffin is not appropriate in cooling wall structure due to flammability. Meanwhile, considering the melting temperature of the PCM should be within the indoor thermal comfortable range 22–26 °C (Rodríguez-Muñoz et al. 2016), inorganic hydrated salt $CaCl_2{\cdot}6H_2O$, which melts at 22 °C, is thus selected and encapsulated in steel containers. Thermo-physical properties of each section of PCMs-VTW system are shown in Table 1.

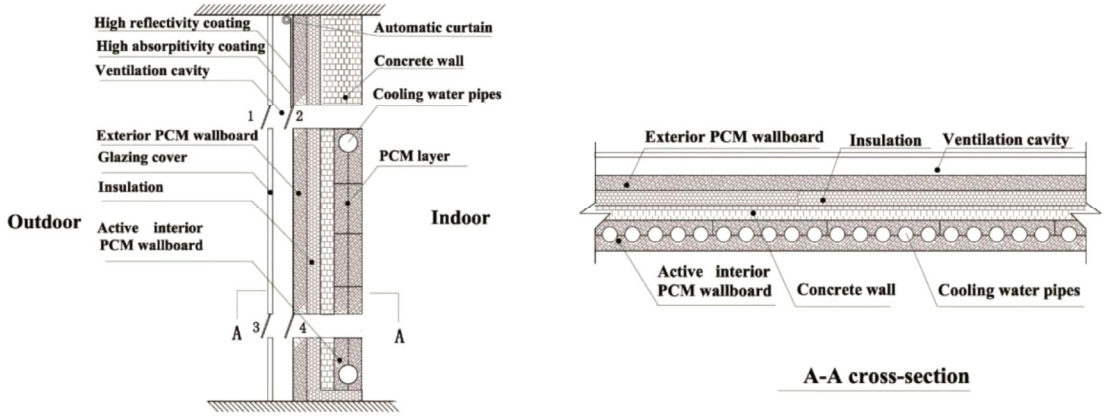

Fig. 1 Detailed construction of the PCMs-VTW system

Table 1 Thermo-physical properties of each section of PCMs-VTW system

Material	Physical properties	Value
Hydrated salt $CaCl_2{\cdot}6H_2O$	ρ	1380 kg/m^3
	$C_{p,s}$	2.53 kJ/(kg·°C)
	$C_{p,l}$	2.53 kJ/(kg·°C)
	H	176 kJ/kg
	Melting temperature of exterior PCM	23 °C
	Thickness of exterior PCM	30 mm
	Melting temperature of interior PCM	22 °C
	Thickness of interior PCM	45 mm
	λ_s	0.5 W/(m·°C)
	λ_l	0.4 W/(m·°C)
	Degree of super-cooling	0.5
	Absorbance of the exterior PCM Wallboard (α_3)	0.6
	Emittance of the interior PCM Wallboard (ε_{12})	0.8
Coating	Reflectivity of coating	0.85
EPS	ρ_e	30 kg/m^3
	λ_e	0.035 w/(m·°C)
	C_e	1.3 kJ/(kg·°C)
	Thickness	10 mm
Brick	C_b	0.75 kJ/(kg·°C)
	ρ_b	2000–2500 kg/m^3
	λ_b	0.39–0.42 W/(m·°C)
	Thickness of interior brick	30 mm
Glass	Emittance (ε_1)	0.92
	Absorbance (α_1)	0.1
	ρ_g	2500 kg/m^3
	C_g	760 kJ/(kg·°C)
	Transmittance (τ_1)	0.85

2.2 System operational strategies

In the PCMs-VTW system, three operational modes are available depending on outdoor weather conditions.

1) Cooling energy storage: air vents 2, 3 are open at night, outdoor air with low temperature enters to air channel from outside, solidifies the exterior PCM and is pumped into room by fans (mechanical ventilation).
2) Cooling energy release: air vents 2, 4 are open at night, indoor air enters air channel, after being cooled down by the PCM, it returns to the chamber. Fan (mechanical ventilation) is used to facilitate cooling energy release in PCM.
3) Natural ventilation at daytime: to avoid overheating at daytime, air vents 1, 3 are open for natural ventilation and the automatic curtain coated by high-reflective coating descends for reflecting solar radiation at daytime.

3 Mathematical model

3.1 Governing equation and boundary conditions

To predict the thermal performance of the proposed system under different climate regions for a relatively long period, numerical model for the buildings fabricated with PCMs-VTW has been developed. Heat transfer equations under each operational state are developed by considering heat transfer of indoor air, heat conduction in the wall, convective heat transfer between channel air and the exterior wall, solar radiation and long wave radiation. In order to develop simplified numerical model without sacrificing the accuracy of the calculation result, some assumptions have been made:

(1) The PCM would be isotropic and homogeneous, meanwhile, convective heat transfer in the melted PCM would be neglected;
(2) Thermo-physical properties of materials would be constant except for the specific heat capacity of PCMs

during melting or freezing process. The effective specific heat capacity would be the average value of the pure solid PCM and the pure liquid PCM during the phrase change process;

(3) Only one-dimensional heat transfer among different layers has been involved.

Energy equations in the internal points could be expressed as below:

In the zone without phase transition:

$$\lambda\frac{\partial}{\partial x}\left(\frac{\partial T}{\partial x}\right)=\rho C\frac{\partial T(r,t)}{\partial t} \tag{1}$$

In the PCM zone:

$$\frac{\partial}{\partial x}\left(\lambda\cdot\frac{\partial T}{\partial x}\right)+\rho\cdot\Delta H\cdot\frac{\mathrm{d}s}{\mathrm{d}t}=\rho\frac{\partial H(r,t)}{\partial t} \tag{2}$$

Figure 2 presents all computational nodes and heat transfer process of three different operational modes. Equations (1) and (2) are solved by proper boundary conditions according to Fig. 2.

As for interior active PCM wallboard, partial differential equation should be discretized differently according to the state of active cooling water.

When the active cooling water is turned on,

$$\frac{\partial}{\partial x}\left(\lambda\cdot\frac{\partial T}{\partial x}\right)=\lambda\frac{T_9^k+T_{\text{lenshui}}^k-2T_{10}^k}{\Delta x^2} \tag{3}$$

$$\frac{\partial}{\partial x}\left(\lambda\cdot\frac{\partial T}{\partial x}\right)=\lambda\frac{T_{12}^k+T_{\text{lenshui}}^k-2T_{11}^k}{\Delta x^2} \tag{4}$$

When the active cooling water is turned off,

$$\frac{\partial}{\partial x}\left(\lambda\cdot\frac{\partial T}{\partial x}\right)=\lambda\frac{T_9^k+T_{11}^k-2T_{10}^k}{\Delta x^2} \tag{5}$$

$$\frac{\partial}{\partial x}\left(\lambda\cdot\frac{\partial T}{\partial x}\right)=\lambda\frac{T_{12}^k+T_{10}^k-2T_{11}^k}{\Delta x^2} \tag{6}$$

Convection with outdoor air, convection with the indoor air and radiation heat transfer with surroundings between external glass and exterior PCM wallboard are simultaneously calculated selectively according to the operational state of the system. At the boundary points of the air channel like 1, 3, 12 and indoor air, heat transfer differential equations are described as follows.

Natural cooling energy storage process at night:

$$\rho_1 C_1\frac{T_1^{k+1}-T_1^k}{\alpha\tau}=\sigma\frac{T_3^{k^4}-T_1^{k^4}}{\frac{1}{\varepsilon_1}+\frac{1}{\varepsilon_3}-1}+h_1(T_{\text{f, wout}}^k-T_1^k)+\varepsilon_1\sigma(T_{\text{eq}}^{k^4}-T_1^{k^4}) \tag{7}$$

$$\rho_{\text{shy}}\frac{H_3^{k+1}-H_3^k}{\alpha\tau}=\sigma\frac{T_1^{k^4}-T_3^{k^4}}{\frac{1}{\varepsilon_1}+\frac{1}{\varepsilon_3}-1}+\lambda_{\text{shy}}\frac{T_4^k-T_3^k}{\Delta x}+h_3(T_{\text{f,wout}}^k-T_3^k) \tag{8}$$

$$(\rho c)_{\text{a}}\frac{T_{\text{f,wout}}^{k+1}-T_{\text{f,wout}}^k}{\alpha\tau}=h_1(T_1^k-T_{\text{f,wout}}^k)+h_3(T_3^k-T_{\text{f,wout}}^k) \tag{9}$$

$$\rho_{\text{shy}}\frac{H_{12}^{k+1}-H_{12}^k}{\Delta\tau}=\lambda_{\text{shy}}\frac{T_{11}^k-T_{12}^k}{\Delta x}+h_{\text{f2}}\left(T_{\text{a}}^k-T_{12}^k\right)+\frac{\sigma(T_{\text{os}}^{k^4}-T_{12}^{k^4})}{\left(\frac{1}{\varepsilon_{12}}-1\right)+\frac{1}{X_{21}}+\frac{F_{12}}{\sum F_i}\left(\frac{1}{\varepsilon_{\text{f}}}-1\right)} \tag{10}$$

$$(\rho c)_{\text{a}}\frac{T_{\text{a}}^{k+1}-T_{\text{a}}^k}{\Delta\tau}=h_{\text{f2}}(T_{12}^k-T_{\text{a}}^k)+\sigma\varepsilon_{12}(T_{12}^{k^4}-T_{\text{a}}^{k^4}) \tag{11}$$

During natural cooling energy storage process, air with low temperature enters the air channel from outside,

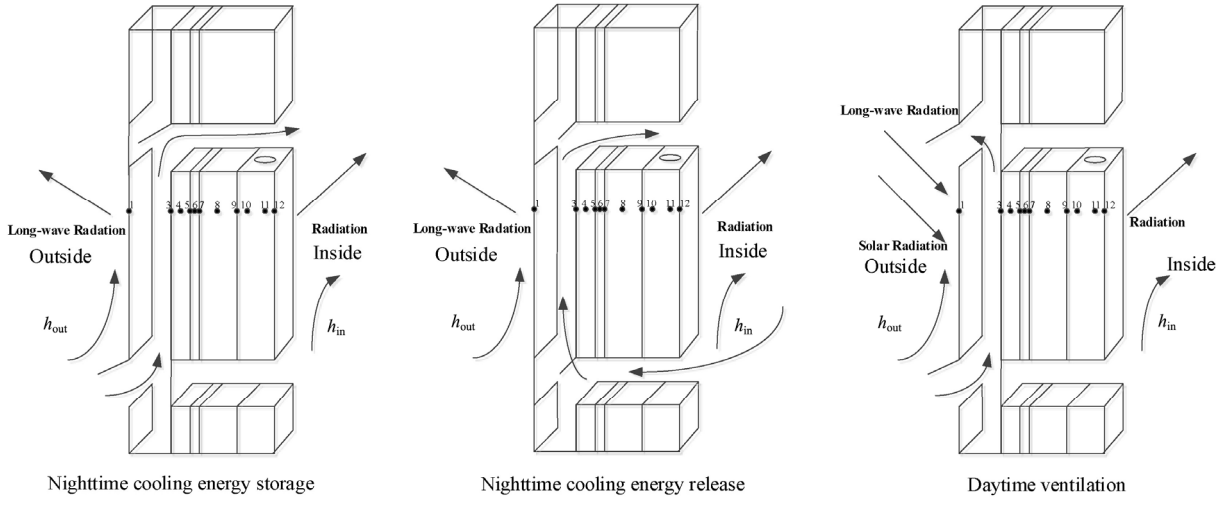

Fig. 2 Computational nodes and heat transfer of three different operational modes

solidifies the PCMs and is pumped into room by fans (mechanical ventilation), being mixed with indoor air. Temperature of the mixed air can be calculated as following:

$$\frac{m_{\mathrm{a,f,out}}}{m_{\mathrm{a,in}}}=\frac{T_{\mathrm{a}}^{k+1}-T_{\mathrm{a}}^{k}}{T_{\mathrm{f,wout}}^{k}-T_{\mathrm{a}}^{k+1}} \tag{12}$$

where $m_{\mathrm{a,f,out}}$ is the mass of the air flowing through the channel [kg/s], which shows positive relationship with the channel airflow rate, $m_{\mathrm{a,in}}$ is the indoor air mass [kg/s].

$$m_{\mathrm{a,f,out}} = \rho\times D\times W\times u \tag{13}$$

$$m_{\mathrm{a,in}} = \rho\times W\times L\times P \tag{14}$$

where D and W are the width and length of the channel [m], respectively, u is the channel airflow rate [m/s], ρ is the air density [kg/m^3], L and P are the width and height of the room [m], respectively.

Also, air change rate could be calculated by

$$n = \frac{t\times D\times W\times u}{W\times L\times P} \tag{15}$$

where t is the ventilated time [s].

Cooling energy release process at night:

$$\rho_1 C_1\frac{T_1^{k+1}-T_1^{k}}{\alpha\tau} = \sigma\frac{T_3^{k^4}-T_1^{k^4}}{\frac{1}{\varepsilon_1}+\frac{1}{\varepsilon_3}-1} +h_1(T_{\mathrm{a}}^{k}-T_1^{k})+\varepsilon_1\sigma\,(T_{\mathrm{eq}}^{k^4}-T_1^{k^4}) \tag{16}$$

$$\rho_{\mathrm{shy}}\frac{H_3^{k+1}-H_3^{k}}{\alpha\tau} = \sigma\frac{T_1^{k^4}-T_3^{k^4}}{\frac{1}{\varepsilon_1}+\frac{1}{\varepsilon_3}-1} +\lambda_{\mathrm{shy}}\frac{T_4^{k}-T_3^{k}}{\Delta x}+h_3(T_{\mathrm{a}}^{k}-T_3^{k}) \tag{17}$$

$$\rho_{\mathrm{shy}}\frac{H_{12}^{k+1}-H_{12}^{k}}{\Delta\tau} = \lambda_{\mathrm{shy}}\frac{T_{11}^{k}-T_{12}^{k}}{\Delta x}+h_{\mathrm{f2}}\left(T_{\mathrm{a}}^{k}-T_{12}^{k}\right) +\frac{\sigma(T_{\mathrm{os}}^{k^4}-T_{12}^{k^4})}{\left(\frac{1}{\varepsilon_{12}}-1\right)+\frac{1}{X_{21}}+\frac{F_{12}}{\sum F_i}\left(\frac{1}{\varepsilon_{\mathrm{f}}}-1\right)} \tag{18}$$

$$(\rho c)_{\mathrm{a}}\frac{T_{\mathrm{a}}^{k+1}-T_{\mathrm{a}}^{k}}{\Delta\tau} = h_{\mathrm{f2}}(T_{12}^{k}-T_{\mathrm{a}}^{k}) +\sigma\varepsilon_{12}(T_{12}^{k^4}-T_{\mathrm{a}}^{k^4})\ +h_1(T_3^{k}-T_{\mathrm{a}}^{k}) \tag{19}$$

Natural ventilation at daytime:

$$\rho_1 C_1\frac{T_1^{k+1}-T_1^{k}}{\alpha\tau} = \sigma\frac{T_3^{k^4}-T_1^{k^4}}{\frac{1}{\varepsilon_1}+\frac{1}{\varepsilon_3}-1} +\alpha_1 I^{k}+h_{\mathrm{w1}}(T_{\mathrm{f,wout}}^{k}-T_1^{k})+\varepsilon_1\sigma\,(T_{\mathrm{eq}}^{k^4}-T_1^{k^4}) \tag{20}$$

$$\rho_{\mathrm{shy}}\frac{H_3^{k+1}-H_3^{k}}{\alpha\tau} = \sigma\frac{T_1^{k^4}-T_3^{k^4}}{\frac{1}{\varepsilon_1}+\frac{1}{\varepsilon_3}-1} +\lambda_{\mathrm{shy}}\frac{T_4^{k}-T_3^{k}}{\Delta x}+\tau_1\alpha_3 I^{k}+h_{\mathrm{w1}}(T_{\mathrm{f,wout}}^{k}-T_3^{k}) \tag{21}$$

$$\rho_{\mathrm{shy}}\frac{H_{12}^{k+1}-H_{12}^{k}}{\Delta\tau} = \lambda_{\mathrm{shy}}\frac{T_{11}^{k}-T_{12}^{k}}{\Delta x}+h_{\mathrm{f2}}\left(T_{\mathrm{a}}^{k}-T_{12}^{k}\right) +\frac{\sigma(T_{\mathrm{os}}^{k^4}-T_{12}^{k^4})}{\left(\frac{1}{\varepsilon_{12}}-1\right)+\frac{1}{X_{21}}+\frac{F_{12}}{\sum F_i}\left(\frac{1}{\varepsilon_{\mathrm{f}}}-1\right)} \tag{22}$$

$$(\rho c)_{\mathrm{a}}\frac{T_{\mathrm{a}}^{k+1}-T_{\mathrm{a}}^{k}}{\Delta\tau} = h_{\mathrm{f2}}(T_{12}^{k}-T_{\mathrm{a}}^{k})+\sigma\varepsilon_{12}(T_{12}^{k^4}-T_{\mathrm{a}}^{k^4}) \tag{23}$$

$$C_{\mathrm{shy}}=\begin{cases}C_{\mathrm{shys}} & T<T_{\mathrm{s}}\\ (C_{\mathrm{shys}}+C_{\mathrm{shyl}})/2 & T_{\mathrm{s}}\le T<T_{\mathrm{l}}\\ C_{\mathrm{shyl}} & T\ge T_{\mathrm{l}}\end{cases} \tag{24}$$

$$\lambda_{\mathrm{shy}}=\begin{cases}\lambda_{\mathrm{shys}} & T<T_{\mathrm{s}}\\ (\lambda_{\mathrm{shys}}+\lambda_{\mathrm{shyl}})/2 & T_{\mathrm{s}}\le T<T_{\mathrm{l}}\\ \lambda_{\mathrm{shyl}} & T\ge T_{\mathrm{l}}\end{cases} \tag{25}$$

where C_{shys} and C_{shyl} are the thermal capacity of PCM in solid and liquid state [kJ/(kg·°C)], respectively; λ_{shys} and λ_{shyl} are thermal conductivity of PCM in solid and liquid state in [W/(m·°C)], respectively; T_{s} and T_{l} are initial melting temperature and completely melting temperature of PCM [°C], respectively.

When the active cooling water pump is turned on, PCM is able to store cooling energy and undergo liquid to solid transformation at certain constant temperature. The solid–liquid interface moves from the center to the two sides of interior PCM wallboard. Heat flux of cooling energy storage is thus calculated by Eq. (26). When active cooling water pump is turned off, indoor air is cooled by PCM, and the solid–liquid interface moves away from indoor surroundings.

$$q_{12}=\frac{T_{\mathrm{m,i}}-T_{\mathrm{in}}}{R_{\mathrm{f2}}+R_{\mathrm{pcm,l}}} \tag{26}$$

$$R_{\mathrm{pcm,l}}=\begin{cases}\dfrac{x_2(t)-(L_1+L_2)}{\lambda_{\mathrm{shyl}}} & \text{cooling water pump is turned on}\\ \dfrac{L_1+L_2+L_3-x_2(t)}{\lambda_{\mathrm{shyl}}} & \text{cooling water pump is turned off}\end{cases} \tag{27}$$

where $T_{\mathrm{m,i}}$ and R_{f2} are the melting temperature of interior PCM [°C] and the heat convective resistance of interior PCM wallboard surface [m^2·°C /W]. $x_2(t)$ is the solid–liquid interface of interior PCM wallboard [m], as a function of

time t. L_1, L_2 and L_3 are the thicknesses of exterior PCM wallboard, medium structure and interior active PCM wallboard [m], respectively. Other parameters are identical with what are aforementioned.

h_{w1} is the heat transfer coefficient of air channel surface under natural ventilation W/(m²·°C), which is determined by:

$$h_{w1} = \frac{Nu_a \cdot \lambda_a}{H} \tag{28}$$

The Nusslet number Nu_a is calculated by Eq. (29) (He et al. 2015; Shen et al. 2007; Hollands et al. 1976):

$$Nu_a = (0.825 + 0.328Ra_a^{1/6})^2 \quad 0.1 < Ra_a < 10^{12} \tag{29}$$

$$Re = \frac{uD}{\nu} \tag{30}$$

$$Pr = \frac{\nu}{a} = 0.7 \tag{31}$$

Re is within the range after calculation: $0 < Re < 2300$

$$Ra_a = \frac{g\beta H^3 \cdot (T_1 - T_a)}{\nu \cdot \alpha} \tag{32}$$

where g is the gravitational acceleration [m/s²], β is the volume expansion coefficient of air [°C⁻¹], ν is the kinematic viscosity of the ventilated air [m²/s], α is the thermal diffusivity coefficient [m²/s].

After calculating Eq. (32) with the condition set by Eq. (29), the $T_1 - T_a$ should be within the range [4.3×10^{-4}, 4.3×10^{9}]. In other words, only when glass surface temperature is higher than air temperature can natural ventilation occur, which is the case at daytime.

h_1 and h_3 are the heat transfer coefficients of glazing surface under mechanical ventilation [W/(m²·°C)], which are determined by Eq. (33) (Welty 1978):

$$h_1 = h_3 = \xi \rho_a C_p u \Delta P^{-2/3}/8 \tag{33}$$

$$\Delta P = \xi \frac{L}{D} \rho_a \frac{u^2}{2g} \tag{34}$$

h_{f2} is the convective heat transfer coefficient for interior PCM wallboard, and is deemed as the constant value 4.8 W/(m²·°C).

T_{os} is the average temperature of other surfaces of the room [°C], F_i is the i-th surface area of the room [m²].

$$T_{os} = \frac{\sum (F_i T_i)}{\sum F_i} \tag{35}$$

T_{eq} is the solar air temperature, which is calculated by:

$$T_{eq} = T_{f,wout} + [\alpha_1 I - Q_{lw}] / h_{out} \tag{36}$$

Compared with the value of solar radiation (I), the value of long wave radiation (Q_{lw}) is too low to be considered during the daytime. However, there is no solar radiation but only long wave radiation at night. Q_{lw} is calculated by following formula:

$$Q_{lw} = \sigma\alpha_1[(X_{sky} + X_g\alpha_g)T_1^4 - X_{sky}T_{sky}^4 - X_g\alpha_g T_g^4] \tag{37}$$

3.2 Solving the numerical model

In this study, governing equation is firstly discretized and then solved by finite difference method (FDM). Central difference (forwards difference) is adopted for central points. Spatial step and time step are 15 mm and 5 s, respectively. All equations are solved by Gaussian iteration. Numerical simulation operated by MATLAB is run according to Fig. 3.

3.3 Validation of the developed numerical model

In order to validate the accuracy of our numerical model, a similar simulation with the same input parameters, i.e. weather condition, dimension parameter and so on, as

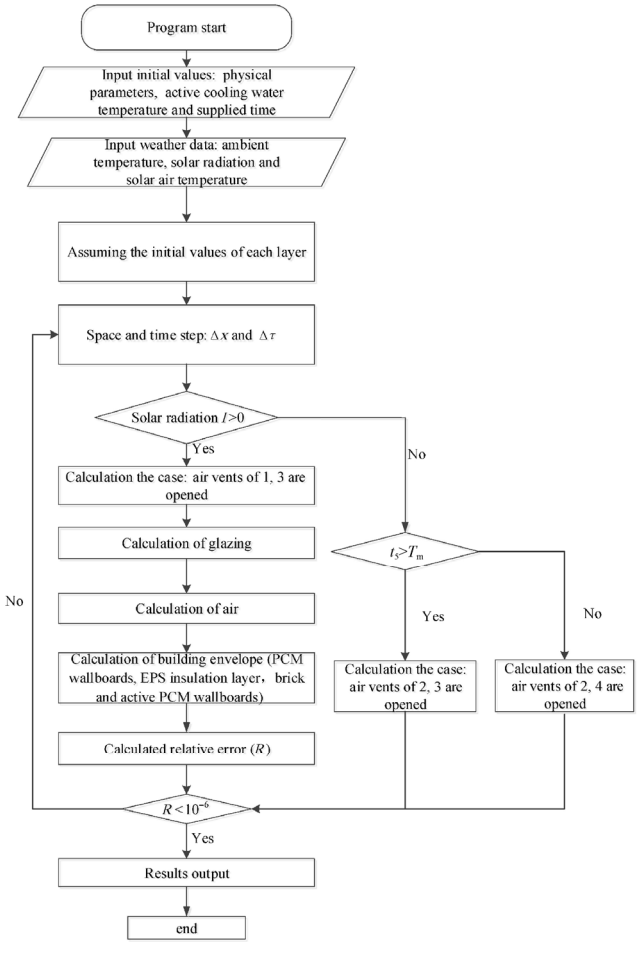

Fig. 3 Flow chart of the computational process

Meng et al. (2013) was carried out on the MATLAB platform. The configuration of the PCMs-VTW room was the same as the Meng et al.'s room except for ventilating air channel in the PCMs-VTW room. More preciously, the dimensions of both rooms were 1000 mm × 1000 mm × 1000 mm. One double glazing window of 670 mm × 670 mm was installed at the south side of each room. Thermos-physical properties are listed in Table 2, and weather profile are kept the same (shown in Fig. 4). Same simulation conditions are ensured between the PCMs-VTW room and Meng et al.'s room via regarding air temperature in air channel and outdoor as the same. Also, the active cooling water pump is off during the whole validation process to create the same condition as Meng et al. (2013).

$$\Delta T_t = T_{\mathrm{Sim},t} - T_{\mathrm{Exp},t} \tag{38}$$

To quantitatively evaluate the accuracy of our modelling, D-value (ΔT) is calculated by subtracting experimental indoor air temperature ($T_{\mathrm{Exp},t}$) from simulation result ($T_{\mathrm{Sim},t}$). The evolution of D-value (ΔT) is shown in Fig. 5. As can be seen in Fig. 5, difference between indoor air temperatures in both rooms is always less than 1. It is obvious that ΔT reaches its peak at midday while it is relatively low at midnight. This is because the thermal inertia of the wall components has not been taken into account in the simulation process. Also, the D-value (ΔT) in PCMs-VTW room is generally lower than the reference room. This is due to low specific thermal capacity in the facade of the reference room. Above all, all simulating results show that our numerical models are reliable and feasible.

Table 2 Thermo-physical properties of double PCMs layers

Materials	T_m(°C)	H (kJ/kg)	C_p (kJ/(kg·°C))	λ (W/(m·°C))	ρ (kg/m^3)
External PCM	28	206	2	0.2	850
Internal PCM	19	225	2	0.2	850

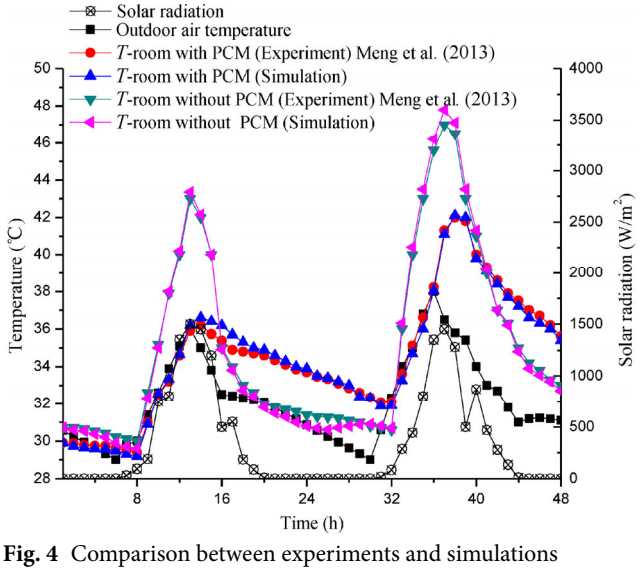

Fig. 4 Comparison between experiments and simulations

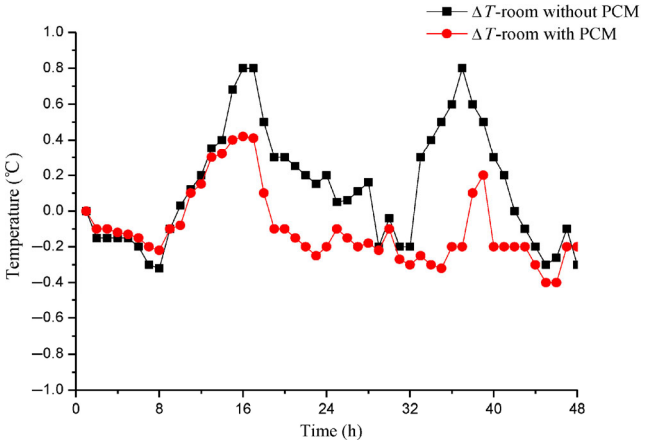

Fig. 5 Evolution of D-value (ΔT) among experiment and simulation in both reference room and PCMs-VTW room

4 Result and discussion

4.1 Effects of melting temperature and latent heat of interior PCM on heat flux

Zhu et al. (2016) pointed out that external PCM layer was active in hot seasons and internal layer was active in cold seasons. Melting temperature of exterior PCM should be higher than nighttime air temperature, which enables the regeneration of solid PCM. It should also be lower than the peak temperature at daytime so as to ensure the melting of PCM. To exclusively evaluate the effect of interior PCM on thermal performance of the whole system, melting temperature of exterior PCM is kept at 23 °C. Both melting temperature and enthalpy of interior PCM are analyzed in detail in this part.

According to design standard of energy efficiency of residential buildings in hot summer and cold winter zone, the cooling period is from June 1st to September 30th and indoor air temperature set-point is 26 °C in summer (Zhu et al. 2015). To quantitatively analyze thermal response of the PCMs-VTW system under typical summer weather condition in Changsha, August 1st to August 7th is selected for our simulation. The weather profile is the typical year data from Chinese Standard Weather Data (CSWD) as shown in Fig. 6. As can been seen in Fig. 6, the average air temperature and solar radiation are 30 °C and 255.5 W/m^2, respectively. According to thermodynamic parameter in Changsha, internal wall surface temperature should not be lower than 19 °C in summer (Olesen 2002).

The active cooling water system is operated according to the scheme shown in Fig. 7. Cooling water is supplied at

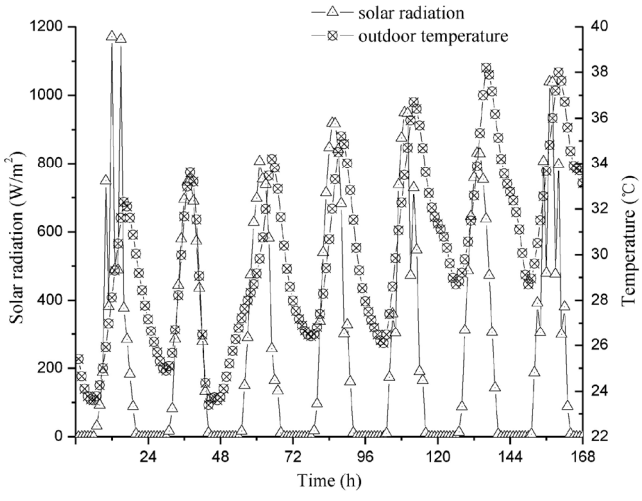

Fig. 6 Solar radiation and outdoor air temperature in Changsha

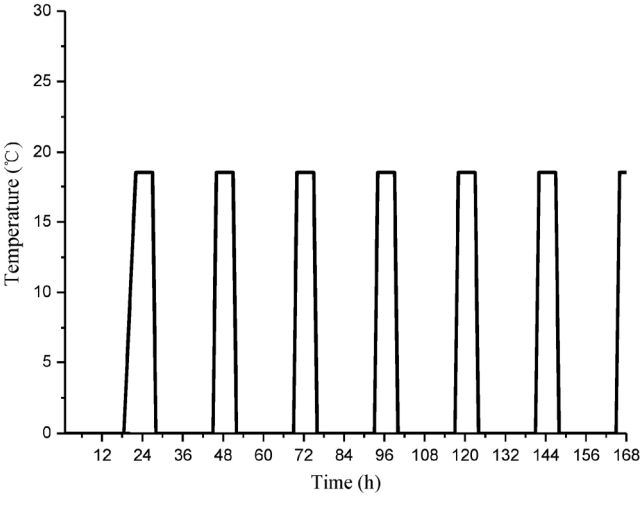

Fig. 7 Operation of active cooling water system

18.5 °C for 6 h every day from 23:00 PM to 5:00 AM (next day) with the variable volume flow rate (q_{sup}), depending on real-time cooling load.

4.1.1 *Effect of PCM's melting temperature on heat flux*

PCM fails to completely melt/solidify when the melting temperature of PCM is too high/low, making the utilization of PCM inadequate. Therefore, it is imperative to identify the appropriate melting temperature of PCM for ensuring discharging (solid PCM) and completely charging (liquid PCM) of PCM, which is highly dependent on local weather condition.

To do this, we evaluate the effect of PCM's melting temperature on heat flux of internal wall surface, which is calculated by Eq. (26). To exclusively evaluate the effect of PCM's melting temperature on heat flux, latent heat of PCM is 176 kJ/kg. As shown in Fig. 8, when the melting temperature is 24 °C or higher, heat flux is almost similar

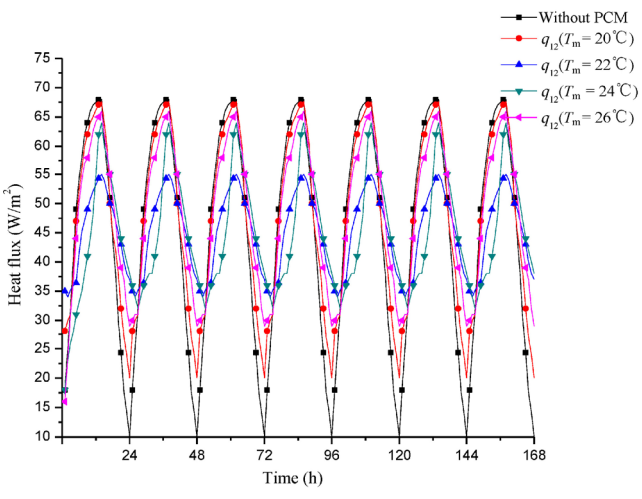

Fig. 8 Effect of the melting temperature on heat flux of internal wall surface (q_{12})

to the wall without PCM. Similarly, if the melting temperature is 20 °C or lower, PCM is unable to completely solidify. The fluctuation of heat flux is the smallest among all cases when the melting temperature of PCM is 22 °C, indicating the efficient charging/discharging of PCM during the process. Table 3 shows the average amount of cooling energy release in each case. In comparison with the room without PCM, cooling energy release increases with different degree by PCM. The maximum average value in cooling energy release reaches 43.5 W/m² when melting temperature of PCM is 22 °C, being increased by 39.4%. In this sense, melting temperature of PCM at 22 °C is more suitable in terms of reducing building cooling load under hot summer condition in Changsha.

4.1.2 *Effect of latent heat of PCM on heat flux*

To evaluate the effect of PCM's enthalpy on heat flux of internal wall surface, heat flux is also calculated by Eq. (26). Similarly, to exclusively evaluate the effect of PCM's latent heat on heat flux, melting temperature of PCM is kept constant at 22 °C. As can be seen in Fig. 9, with the increase in latent heat of PCM, internal wall surface heat flux (q_{12}) is more stable, indicating the efficient charging/discharging of PCM. It should be noted that in comparison with the room without PCM, room with PCM could still provide a relatively high cooling energy after the cooling water pump is turned off. Table 4 shows average amount in cooling

Table 3 Average amount of cooling energy release among different melting temperature of PCM

	Without PCM	T_m=20 °C	T_m=22 °C	T_m=24 °C	T_m=26 °C
Cooling energy release (W/m²)	31.2	38	43.5	40.2	38
Increase (%)	0	22.4	39.4	28.8	21.8

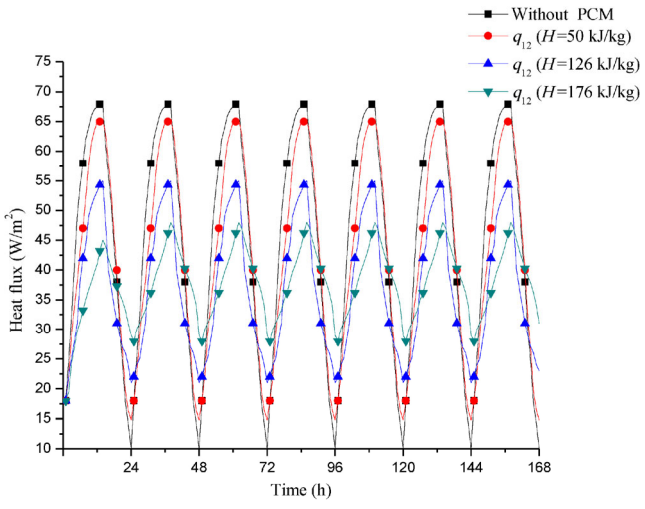

Fig. 9 Effect of latent heat of PCM on heat flux of internal wall surface (q_{12})

Table 4 Average amount of energy release among different latent heat of PCM

	Without PCM	H=50 kJ/kg	H=126 kJ/kg	H=176 kJ/kg
Energy release (W/m^2)	31.2	34.8	41	44.2
Increase (%)	0	11.5	31.4	41.7

energy release for PCMs with different latent heat. In comparison with the room without PCM, the maximum average cooling energy release is 44.2 W/m^2 when the latent heat of PCM is 176 kJ/kg, being increased by 41.7%. In this sense, latent heat of PCM at 176 kJ/kg is more suitable in terms of reducing building cooling load under hot summer condition in Changsha.

4.1.3 Evolution of indoor air temperature for different latent heat of PCMs

Figure 10 indicates temperature evolution of glazing layer (T_1), exterior PCM wallboard surface (T_3), internal wall surface (T_{12}) and indoor air (T_a) for different latent heat of PCM. As can been seen in Fig. 10(a), temperature of glazing layer increases with the increase in solar radiation, while it decreases at night due to low outdoor temperature and long wave radiation. As for exterior PCM wallboard, it is noteworthy that PCM fails to store natural cooling energy at night when latent heat of PCM is 126 kJ/kg as the temperature of the exterior PCM wallboard surface is always higher than its melting temperature except for the initial 36 h. When latent heat of PCM is increased to 176 kJ/kg, PCM could solidify to store natural cooling energy at night (when T_3 decreases below 22 °C) and release the energy (when T_3 increases above 22°C). However, there is an increasing trend for T_3, indicating the overheating of exterior PCM wallboard. With regard to Fig. 10(b), interior active PCM wallboard surface temperature (T_{12}) is more stable when the latent heat of PCM is increased from 126 kJ/kg to 176 kJ/kg. As a result, indoor air temperature is kept within a narrower range with the increase in latent heat of PCM.

4.2 Comparisons between room with PCMS-VTW, room with VTW and that with classic Trombe wall

In order to evaluate and emphasize the thermal performance of the PCMs-VTW system, comparative study based on three different rooms: room with PCMs-VTW, room with VTW (similar to the former room in configuration except for no PCM in this room) and room with classic Trombe wall, have been conducted based on our modelling. Melting temperature and latent heat of PCM are 22 °C and 176 kJ/kg, respectively. Cooling water is supplied under the scheme shown in Fig. 7.

Figure 11 shows evolution of indoor air temperature for three rooms (with PCMs-VTW, with VTW and with classical Trombe wall). As can been seen in Fig. 11, average

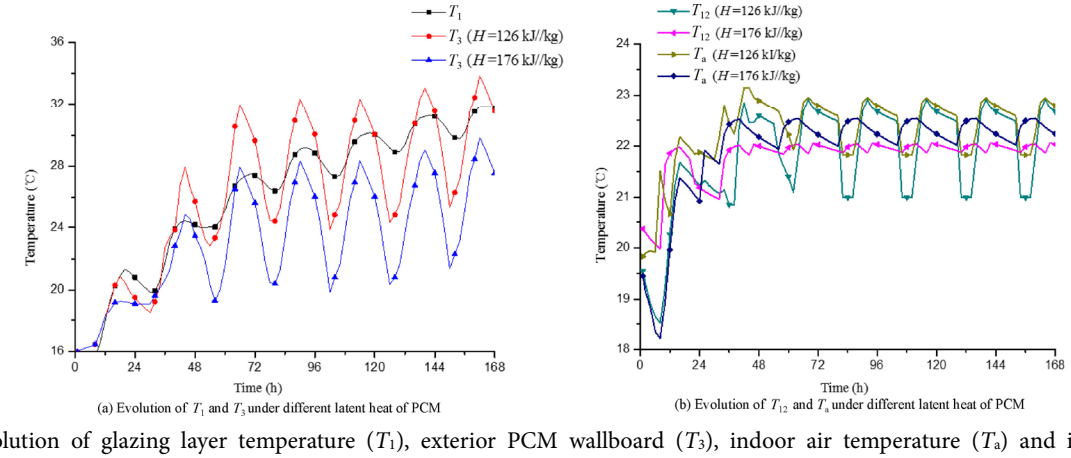

(a) Evolution of T_1 and T_3 under different latent heat of PCM

(b) Evolution of T_{12} and T_a under different latent heat of PCM

Fig. 10 Evolution of glazing layer temperature (T_1), exterior PCM wallboard (T_3), indoor air temperature (T_a) and interior PCM wallboard surface (T_{12}) under different latent heat of PCM

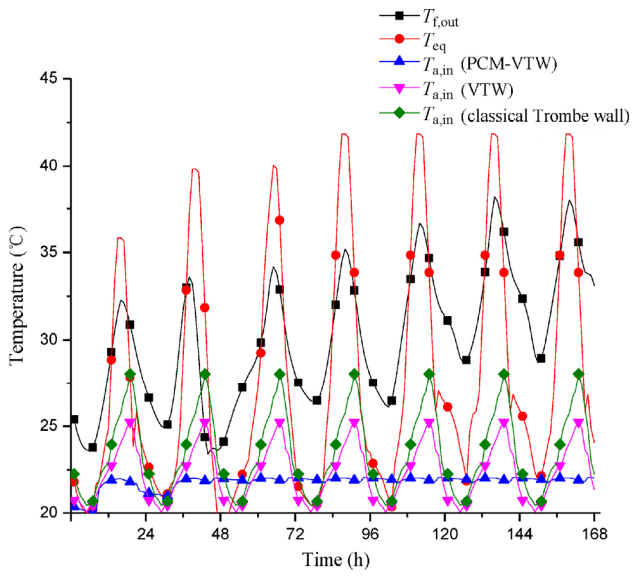

Fig. 11 Indoor air temperature in the room with PCMs-VTW, room with VTW and that with classical Trombe wall

indoor air temperature is 21 °C in the room with PCMs-VTW, while 22 °C for the room with VTW and 24 °C for room with classical Trombe wall. It indicates that under identical cooling water supply scheme, average indoor air temperature is kept at a lower value in the PCMs-VTW system in comparison with other two cases. Moreover, maximum indoor air temperature of the room with VTW and room with classical Trombe wall are 25.25 °C and 28.05 °C, being decreased by nearly 3 °C due to the implementation of radiant cooling system. It should also note that indoor air temperature in PCMs-VTW room is almost kept at constant value, 21.75 °C, reducing indoor air temperature fluctuation range and thus improving local comfort for occupants (Trebilcock et al. 2017) because of the adoption of PCM layer.

In other words, if average indoor air temperature is kept the same for the three cases, requirement in cooling energy, i.e. cooling water temperature as well as its supply time, will be greatly decreased in the PCMs-VTW system. Total cooling energy is calculated by Eq. (39).

$$Q_{sup} = C_{sup} \cdot \rho \cdot \sum q_{sup,t} \cdot \Delta\tau \cdot (T_{sup,t} - T_{ret,t}) \quad (39)$$

Table 5 shows the annual cooling energy consumption and its percentage reduction in the three different cases when indoor air set temperatures are kept at 22 °C and 24 °C respectively. Clearly, maximum reduction in annual cooling energy consumption is in PCMs-VTW fabricated room. Specifically, annual cooling energy consumption is decreased by 20.8% related to the room with classic Trombe wall when indoor air set temperature is 22 °C, and annual cooling energy consumption is decreased by 18.6% when indoor air set temperature is 24 °C in the PCMs-VTW room. In the PCMs-VTW system, the larger percentage reduction in annual cooling energy consumption is due to the larger amount in cooling energy when indoor air set temperature is lower.

4.3 Comparisons between PCM wallboard coated with high-reflective coating and that with no coating

Although the increase in latent heat of PCM is beneficial for mitigating exterior PCM overheating problem, an increasing trend in the temperature of exterior PCM wallboard is unavoidable, as mentioned in Section 4.1.3, causing overheating of exterior PCM wallboard after several continuous charging/discharging processes of PCM. To mitigate overheating problem, many researches have focused on the application of shading devices in the air gap of the Trombe wall to decrease the temperature of exterior wall surface (Baldinelli 2009; Ji et al. 2007). Although cooling energy consumption was reduced by the application of shading devices, electrical consumption of mechanical fan increased with the increase in tilt angle of shading device due to the increase in flow resistance. In order to simultaneously decrease energy consumption of mechanical fan and mitigate overheating of the exterior wall, high-reflective coating with reflectivity at 0.85 is coated on exterior PCM wallboard surface to reflect solar radiation. A large amount of solar radiation is reflected instead of transmitting through the wall in summer.

Figure 12 shows temperature evolution of both exterior PCM wallboard and indoor air with and without high-reflective coating. As can be seen in Fig. 12, in comparison with the system without high-reflective coating, the maximum

Table 5 Annual cooling energy consumption and its percentage reduction in three different cases under different indoor set temperature

	Base temperature (22 °C)		Base temperature (24 °C)	
	Annual cooling energy consumption (kWh)	Percentage of cooling energy consumption reduction (%)	Annual cooling energy consumption(kWh)	Percentage of cooling energy consumption reduction (%)
Classical Trombe wall	553	0	522	0
VTW	493	10.8	472	9.6
PCMs-VTW	438	20.8	425	18.6

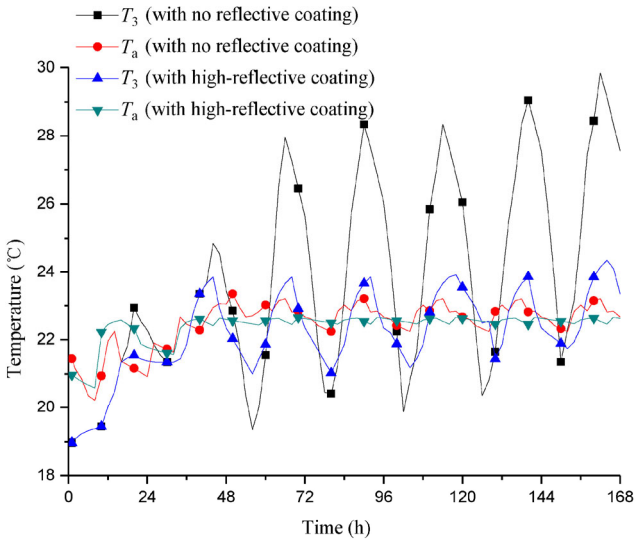

Fig. 12 Temperature evolution of exterior PCM wallboard and indoor air in the room with and without reflective coating

temperature of exterior PCM wallboard surface (T_3) is lowered by 6 °C in the high-reflective coating case. By contrast, in the system without high-reflective, exterior PCM wallboard coating has the tendency to be overheated after several charging/discharging processes, failing to store cooling energy in that case. As for indoor air temperature, it is almost constant in the room with high-reflective coating while there is still 2 °C temperature fluctuation range in the room without high-reflective coating.

4.4 Effect of airflow rate on the regeneration of exterior PCM for room with/without high-reflective coating

In order to investigate the effect of airflow rate on regeneration of exterior PCM, temperature of exterior PCM wallboard (T_3) with and without high-reflective coating was captured and plotted. As can be seen in Fig. 13(a), the regeneration period for exterior PCM is extended with the increase in airflow rate. Specifically, time for exterior PCM regeneration is extended from 54 h to 102 h when airflow rate increases from 1 m/s to 7 m/s. It should note that exterior PCM temperature undergoes sudden increase after finishing completely charging process. This is because that latent heat of PCM is fully utilized and the amount of sensible heat could not be compared with its latent heat. It should also note that although overheating of the external PCM wallboard is mitigated by ventilation depending on airflow rate, an overheating trend of exterior PCM is still unavoidable, causing the inadequate utilization of PCM.

With regard to Fig. 13(b), time for exterior PCM regeneration is dramatically increased by adopting high-reflective coating. In comparison with the case without high-reflective coating, time for exterior PCM regeneration is extended from 54 h to around 108 h when the airflow rate is 1 m/s. It should also note that the exterior PCM is able to actualize complete regeneration during the simulation process when the airflow rate is 7 m/s.

4.5 Effect of airflow rate on indoor air temperature of the room with and without high-reflective coating

To investigate the effect of airflow rate on indoor air temperature, indoor air temperature (T_a) in the room with and without high-reflective coating was captured and plotted. As can be seen in Fig. 14(a), indoor air temperature fluctuation range is narrowed with the increase in airflow rate. Specifically, indoor air temperature fluctuation range is reduced from 11 °C to 3.7 °C when airflow rate increases from 1 m/s to 7 m/s. Moreover, with regard to indoor thermal comfort, indoor air temperature is maintained within the ASHRAE comfort zone (22 °C – 26 °C) in summer for 152 h, 128 h, 118 h and 109 h when airflow rate is 7 m/s,5 m/s,3 m/s and 1 m/s, respectively.

With regard to Fig. 14(b), temperature fluctuation range could be, to some extent, decreased with the implementation of high-reflective coating. In comparison with the case without high-reflective coating, temperature fluctuation

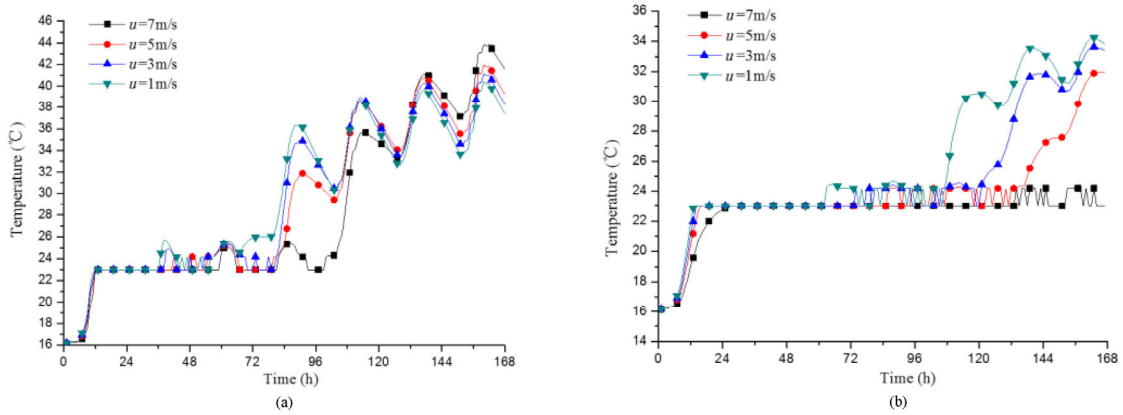

Fig. 13 Evolution of exterior PCM wallboard temperature (T_3): (a) without high-reflective coating; (b) with high-reflective coating

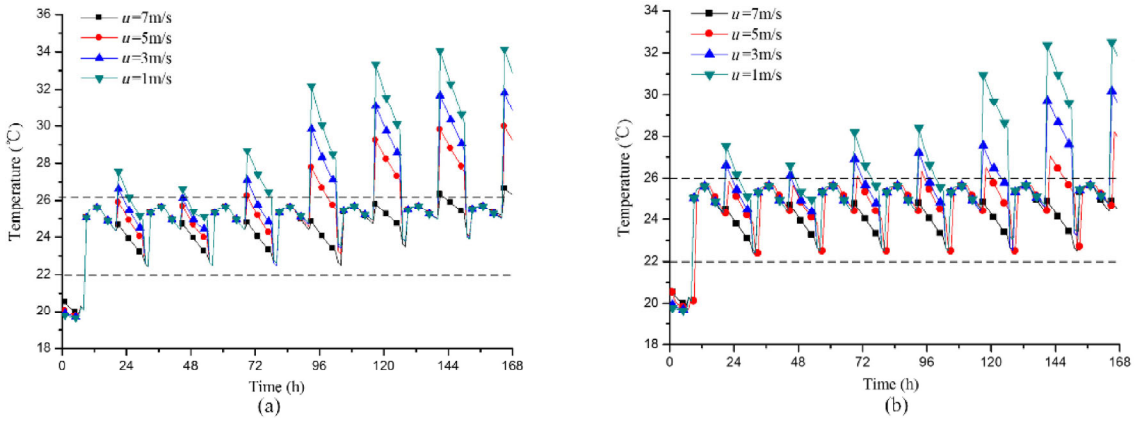

Fig. 14 Evolution of indoor air temperature (T_a): (a) without high-reflective coating; (b) with high-reflective coating

range is reduced from 11 °C to 8.2 °C when airflow rate is 1 m/s. Moreover, indoor air temperature could be maintained within the ASHRAE comfort zone (22 °C – 26 °C) in summer for 160 h, 145 h, 128 h and 115 h when airflow rate was 7 m/s, 5 m/s, 3 m/s and 1 m/s, respectively.

4.6 Thermal performance evaluation of PCMs-VTW system under different weather conditions

To investigate the thermal performance of the PCMs-VTW system under different weather conditions, simulation study has been conducted among typical cities in different climate regions in China. The selected cities are Yan'an, Lasa, Kunming and Haikou, which corresponds to the cold area, extreme cold area, mild climate region and hot summer and warm winter zone, respectively. The input of the simulation are solar radiation and ambient temperature, as shown in Fig. 15. As can been seen in Fig. 15, for the selected cities, average air temperature are 23 °C, 15.6 °C, 20.5 °C and 28.4 °C, meanwhile, solar radiation during the selected period are 205.4 W/m^2, 293.14 W/m^2, 224.6 W/m^2 and 242.4 W/m^2, respectively. Meanwhile, active cooling water is supplied at 18.5 °C for 6 h every day from 23:00PM to 5:00AM as shown in Fig. 7.

As can be seen in Fig. 16, in Kunming (mild climate area), indoor air temperature is maintained at the comfort

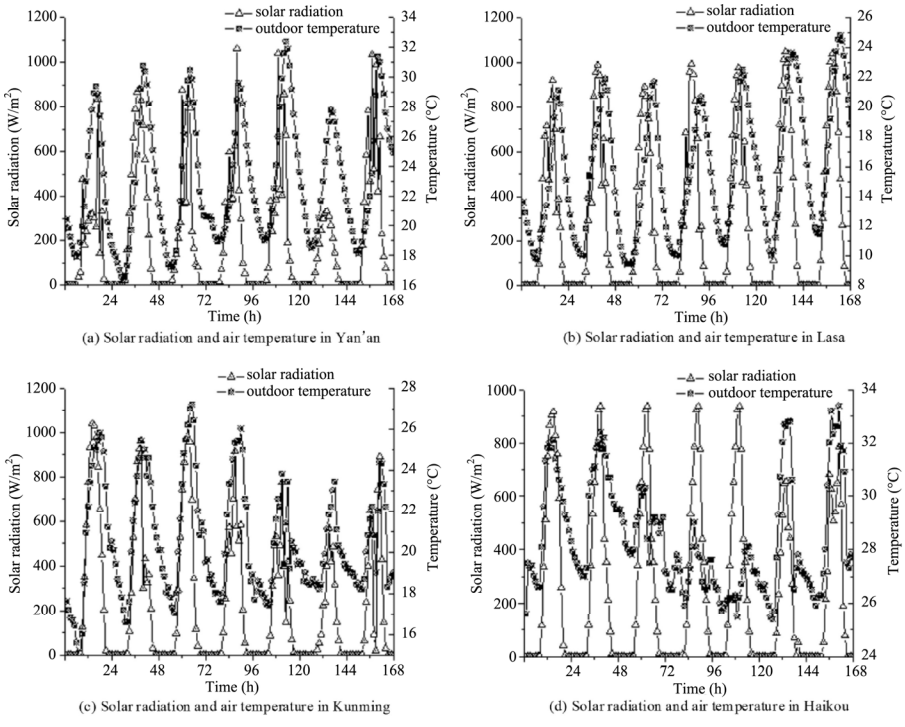

Fig. 15 Solar radiation and outdoor air temperature in the four different climate regions in China: (a) Yan'an (cold area); (b) Lasa (extreme cold area); (c) Kunming (mild climate region); (d) Haikou (hot summer and warm winter zone)

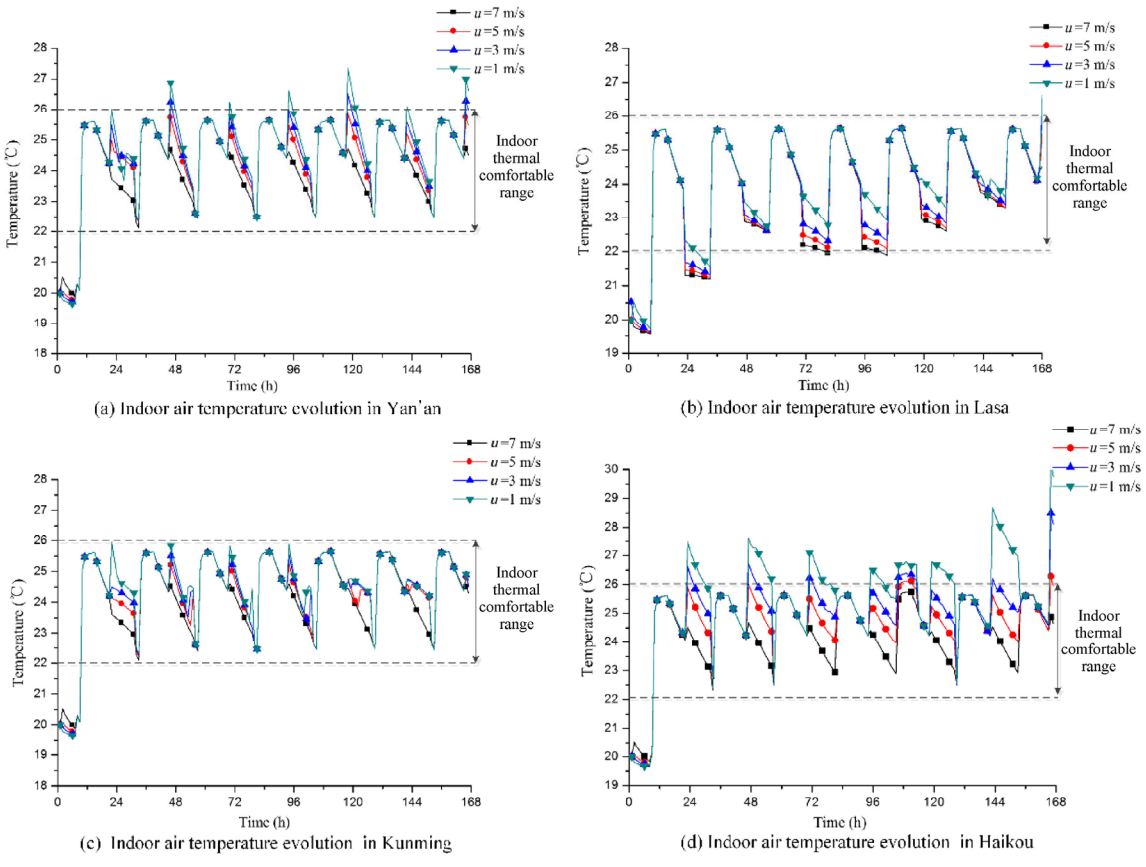

Fig. 16 Evolution of indoor air temperature (T_a): (a) Yan'an (cold area); (b) Lasa (extreme cold area); (c) Kunming (mild climate region); (d). Haikou (hot summer and warm winter zone)

zone all the time except for the initial period. Also, Lasa (extreme cold area) is the only city that indoor air temperature appears to be below 22 °C due to its low ambient temperature.

To further quantitatively evaluate indoor air temperature within thermal comfort range, hours within the comfort zone are calculated in each case as shown in Table 6. As can be seen in Table 6, period for indoor air temperature within thermal comfort range decreases with the decrease in airflow rate while completely contrary trend is in Lasa. This is because that, in extreme cold region, mixing with outdoor air leads indoor air temperature below 22 °C, as shown in Fig. 16(b). It should also note that increasing airflow rate is more effective in increasing indoor air comfortable period in Haikou than other cities. More specifically, in comparison with Yan'an (from 145 h to 159 h), hours for indoor air temperature within thermal comfort range increases from 96 h to 159 h in Haikou when airflow rate increases from 1 m/s to 7 m/s. It should also note that Kunming is the only city that hours for indoor air temperature within thermal comfort range is kept constant (159 h), which is independent on airflow rate. This is because of the mild ambient temperature in Kunming.

Table 6 Hours for indoor air temperature within thermal comfort range in different climate regions in China

Airflow rate (m/s)	Air change rate (times/h)	Hours for indoor air temperature within thermal comfort range			
		Yan'an	Lasa	Kunming	Haikou
7	56	159	142	159	159
5	40	158	148	159	151
3	24	154	148	159	138
1	8	145	152	159	96

4.7 Discussion and limitations

The limitation of our research is that only 12 nodes are adopted for investigating thermal performance of the PCMs-VTW system, which is the main source of inaccuracy and errors. To quantitatively evaluate the effect of nodes' number on our simulation results, comparative study on different nodes has been carried out given relative error (RE) and root mean square error (RMSE), which are shown in Eq. (40) and (41). It should note that in terms of nodes' distribution, only one node is in glass, other nodes are proportionally distributed according to the nodes distribution as shown

in Fig. 2.

$$RE_{Exp,i} = \frac{|\Delta T_t|}{T_{Exp,t}} \times 100\% \quad (40)$$

$$\text{Total relative error} = \sum_{t=1}^{t_{end}} RE_{Exp,t}$$

$$\text{Average relative error} = \text{Total relative error}/(t_{end}-1)/\tau$$

$$RMSE = \sqrt{\frac{\sum_{t=1}^{t_{end}}(T_{Exp,t} - T_{Sim,t})^2}{(t_{end}-1)/\tau}} \times 100\% \quad (41)$$

As can be seen in Fig. 17, when the total number of nodes is 12, average relative error and RMSE are 0.78% and 34.5%, respectively for the system without PCM while 0.59% and 22.7% for the system with PCM. It should note that both relative error and RMSE decrease with the increase in total simulation nodes. More specifically, with the rise in total number of nodes from 12 to 28, total relative error in the system without PCM decreases from 37.5% to 17%, and correspondingly, average relative error decreases from 0.78% to 0.35%. RMSE decreases from 34.5% to 15.7%. Simultaneously, lower relative error is seen in system with PCM, which decreases from 28.2% to 12.7% in total relative error and decreases from 0.59% to 0.27% in average relative error. RMSE decreases from 22.7% to 10.3%. It should also note that magnitude in relative errors decrease drops with the further increase in total number of nodes. It is predicted that with the further increase in total number of simulation nodes, both relative error and RMSE will be close to a constant value.

Another limitation of our research is that internal heat gains from lighting, equipment and occupants are not taken into account for evaluating the feasibility of free-cooling in our system. Also, the peak loading shifting via heat storage of PCM is not yet demonstrated. Apart from this, absorbance of the glass changes constantly with the change in incidence light angle, while only constant value is adopted in our simulation. Moreover, only one-dimensional numerical modelling is developed without taking temperature difference along the vertical and axial directions. Based on this, our future research will mainly focus on quantitatively evaluating cooling cost saving of our system taking internal gains into account. Meanwhile, we will adopt time-dependent absorbance for glass, and concentrate on developing three-dimensional models for our future research.

5 Conclusion

A new ventilated Trombe wall integrated with active PCM encapsulated wallboard has been proposed. Thermal performance of the system has been investigated in this study. Double PCM wallboards are adopted for different purposes, i.e. the exterior PCM wallboard is for the improvement in natural cooling energy storage efficiency, the interior one is for radiant cooling. High-reflective coating as well as natural ventilation is turned out to be effective in ameliorating overheating at daytime. Meanwhile, natural cooling energy storage efficiency is improved with the application of mechanical ventilation at night. A dynamic model has been developed to evaluate thermal performance of the room fabricated with the PCMs-VTW system, which is used for evaluating its feasibility among typical cities in different climate regions in China from 1st August to 7th August, especially in Changsha. Furthermore, comparative study among room with PCM-VTW, room with VTW and that with classical Trombe wall has been conducted. Based on the results, some conclusions can be drawn as follows:

1) The new PCMs-VTW system is effective in maintaining indoor air temperature within thermal comfortable zone in severe summer condition. Overheating problem at midday could be mitigated by coating high-reflective

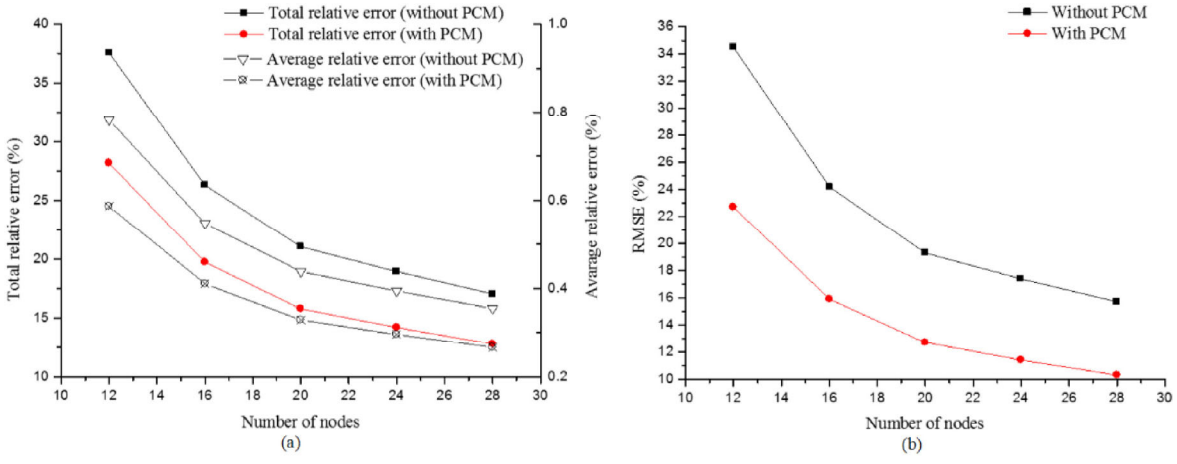

Fig. 17 Relative error and RMSE for different simulation nodes

coating on the surface of exterior PCM wallboard as well as activating natural ventilation.

2) By conducting comparative study according to weather condition in Changsha, melting temperature 22 °C for interior PCM actualizes relatively higher average cooling energy release, 43.5 W/m^2, being increased by 39.4% in comparison with the case lacking of PCM. Similarly, latent heat of exterior PCM 176 kJ/kg contributes to 44.2 W/m^2 in average cooling energy release, being increased by 41.7% compared with the case lacking of PCM.
3) Compared with classical Trombe wall system, when indoor air set temperature is 22 °C in the PCMs-VTW system, annual cooling energy consumption is 438 kWh, which is decreased by 20.8%; when indoor air set temperature is 24 °C, it is 425 kWh, being decreased by 18.6%.
4) Increasing airflow rate and adopting high-reflective coating are validated to be effective ways in terms of enhancing the regeneration of solid exterior PCM wallboard. More specifically, in comparison with the case without high-reflective coating, time for exterior PCM regeneration could be extended from 54 h to around 108 h when airflow rate is 1 m/s. Moreover, complete regeneration of exterior PCM is possible during the whole simulation process when airflow rate is 7 m/s.
5) Except for Lasa (extreme cold region), hours for indoor air temperature within thermal comfort range increases with the increase in airflow rate. Specifically, with the increase in airflow rate from 1 m/s to 7 m/s, the most obvious increase in period for indoor air temperature within thermal comfort range is in Haikou (from 96 h to 159 h), followed by Yan'an (from 145 h to 159 h).

The feasibility of the PCMs-VTW system in severe summer condition is validated by aforementioned conclusions. The dynamic numerical model developed in this study could be effective in predicting thermal behavior and optimizing both geometric and operational parameters of the PCMs-VTW system. Experimental set-up will be established and onsite measurements are needed to provide more accurate evaluation of its efficiency in the near future.

Acknowledgements

This study was supported by the International Science & Technology Cooperation Program of China (No. 2014DFE70230, No. 2014DFA72190).

References

ASHRAE (2007). ASHRAE 62.1. Ventilation for Acceptable Indoor Air Quality. Atlanta, GA, USA: American Society of Heating, Refrigerating and Air-Conditioning Engineers.

Baldinelli G (2009). Double skin facades for warm climate regions: Analysis of a solution with an integrated movable shading system. *Building and Environment*, 44: 1107–1118.

Bellos E, Tzivanidis C, Zisopoulou E, Mitsopoulos G, Antonopoulos KA (2016). An innovative Trombe wall as a passive heating system for a building in Athens—A comparison with the conventional Trombe wall and the insulated wall. *Energy and Buildings*, 133: 754–769.

Bourne S, Novoselac A (2015). Compact PCM-based thermal stores for shifting peak cooling loads. *Building Simulation*, 8: 673–688.

Borreguero AM, Sánchez ML, Valverde JL, Carmona M, Rodríguez JF (2011). Thermal testing and numerical simulation of gypsum wallboards incorporated with different PCMs content. *Applied Energy*, 88: 930–937.

Cao S, Sirén K (2014). Impact of simulation time-resolution on the matching of PV production and household electric demand. *Applied Energy*, 128: 192–208.

Cao S, Sirén K (2015). Matching indices taking the dynamic hybrid electrical and thermal grids information into account for the decision-making of nZEB on-site renewable energy systems. *Energy Conversion and Management*, 101: 423–441.

Chen B, Chen X, Ding YH, Jia X (2006). Shading effects on the winter thermal performance of the Trombe wall air gap: An experimental study in Dalian. *Renewable Energy*, 31: 1961–1971.

de Gracia A, Navarro L, Castell A, Cabeza LF (2013). Numerical study on the thermal performance of a ventilated facade with PCM. *Applied Thermal Engineering*, 61: 372–380.

Feng H, Tian X, Cao S, Zhao J, Deng S (2016). Match performance analysis for a solar-driven energy system in net zero energy building. *Energy Procedia*, 88: 394–400.

Fiorito F (2012). Trombe walls for lightweight buildings in temperate and hot climates. Exploring the use of phase-change materials for performances improvement. *Energy Procedia*, 30: 1110–1119.

Ghrab-Morcos N, Bouden C, Franchisseur R (1993). Overheating caused by passive solar elements in Tunis. Effectiveness of some ways to prevent it. *Renewable Energy,* 3: 801–811.

Gan G (1998). A parametric study of Trombe walls for passive cooling of buildings. *Energy and Buildings*, 27: 37–43.

Hernández-López I, Xamán J, Chávez Y, Hernández-Pérez I, Alvarado-Juárez R (2016). Thermal energy storage and losses in a room-Trombe wall system located in Mexico. *Energy*, 109: 512–524.

Hu Z, He W, Hong X, Ji J, Shen Z (2016). Numerical analysis on the cooling performance of a ventilated Trombe wall combined with venetian blinds in an office building. *Energy and Buildings,* 126: 14–27.

Hernández-Pérez I, Xamán J, Macías-Melo EV, Aguilar-Castro KM, Zavala-Guillén I, Hernández-López I, Simá E (2018). Experimental thermal evaluation of building roofs with conventional and reflective coatings. *Energy and Buildings*, 158: 569–579.

Halawa E, van Hoof J, Soebarto V (2014). The impacts of the thermal radiation field on thermal comfort, energy consumption and control—A critical overview. *Renewable and Sustainable Energy Reviews*, 37: 907–918.

He W, Hu Z, Luo B, Hong X, Sun W, Ji J (2015). The thermal behavior of Trombe wall system with venetian blind: An experimental and numerical study. *Energy and Buildings,* 104: 395–404.

Hollands KGT, Unny TE, Raithby GD, Konicek L (1976). Free convective heat transfer across inclined air layers, *Journal of Heat Transfer*, 98: 189–193.

Ji Jie, Yi H, He W, Pei G (2007). PV-Trombe wall design for buildings in composite climates. *Journal of Solar Energy Engineering*, 129: 431–437.

Joudi A, Svedung H, Cehlin M, Rönnelid M (2013). Reflective coatings for interior and exterior of buildings and improving thermal performance. *Applied Energy*, 103: 562–570.

Khalifa AJN, Abbas EF (2009). A comparative performance study of some thermal storage materials used for solar space heating. *Energy and Buildings*, 41: 407–415.

Krüger E, Suzuki E, Matoski A (2013). Evaluation of a Trombe wall system in a subtropical location. *Energy and Buildings*, 66: 364–372.

Le Dréau J, Heiselberg P, Jensen RL (2015). A full-scale experimental set-up for assessing the energy performance of radiant wall and active chilled beam for cooling buildings. *Building Simulation*, 8: 39–50.

Mavrigiannaki A, Ampatzi E (2016). Latent heat storage in building elements: A systematic review on properties and contextual performance factors. *Renewable and Sustainable Energy Reviews*, 60: 852–866.

Meggers F, Guo H, Teitelbaum E, Aschwanden G, Read J, Houchois N, Pantelic J, Calabrò E (2017). The Thermoheliodome—"Air conditioning" without conditioning the air, using radiant cooling and indirect evaporation. *Energy and Buildings*, 157: 11–19.

Meng E, Yu H, Zhan G, He Y (2013). Experimental and numerical study of the thermal performance of a new type of phase change material room. *Energy Conversion and Management*, 74: 386–394.

Mikeska T, Fan J, Svendsen S (2017). Full scale measurements and CFD investigations of a wall radiant cooling system integrated in thin concrete walls. *Energy and Buildings*, 139: 242–253.

Nikoofard S, Ugursal V I, Beausoleil-Morrison I (2015). Techno-economic assessment of the impact of phase change material thermal storage on the energy consumption and GHG emissions of the Canadian Housing Stock. *Building Simulation*, 8: 225–238.

Ning B, Chen Y, Liu H, Zhang S (2016). Cooling capacity improvement for a radiant ceiling panel with uniform surface temperature distribution. *Building and Environment*, 102: 64–72.

Olesen BW (2002). Radiant floor heating in theory and practice. *ASHRAE Journal*, 44(7): 19–24.

Rabani M, Kalantar V, Dehghan AA, Faghih AK (2015a). Experimental study of the heating performance of a Trombe wall with a new design. *Solar Energy*, 118: 359–374.

Rabani M, Kalantar V, Dehghan AA, Faghih AK (2015b). Empirical investigation of the cooling performance of a new designed Trombe wall in combination with solar chimney and water spraying system. *Energy and Buildings*, 102: 45–57.

Romaní J, Pérez G, de Gracia A (2016). Experimental evaluation of a cooling radiant wall coupled to a ground heat exchanger. *Energy and Buildings*, 129: 484–490.

Romaní J, Cabeza LF, Pérez G, Pisello AL, de Gracia A (2018a). Experimental testing of cooling internal loads with a radiant wall. *Renewable Energy*, 116: 1–8.

Romaní J, Cabeza LF, de Gracia A (2018b). Development and experimental validation of a transient 2D numeric model for radiant walls. *Renewable Energy*, 115: 859–870.

Rodríguez-Muñoz NA, Nájera-Trejo M, Alarcón-Herrera O, Martín-Domínguez IR (2016). A buildings thermal assessment using dynamic simulation. *Indoor and Built Environment,* https://doi.org/10.1177/1420326X16668568.

Sharma A, Tyagi VV, Chen CR, Buddhi D (2009). Review on thermal energy storage with phase change materials and applications. *Renewable and Sustainable Energy Reviews*, 13: 318–345.

Soares N, Reinhart C F, Hajiah A (2017). Simulation-based analysis of the use of PCM-wallboards to reduce cooling energy demand and peak-loads in low-rise residential heavyweight buildings in Kuwait. *Building Simulation,* 10: 481–495.

Saadatian O, Sopian K, Lim CH, Asim N, Sulaiman MY (2012). Trombe walls: A review of opportunities and challenges in research and development. *Renewable and Sustainable Energy Reviews*, 16: 6340–6351.

Shen J, Lassue S, Zalewski L, Huang D (2007). Numerical study on thermal behavior of classical or composite Trombe solar walls. *Energy and Buildings*, 39: 962–974.

Shen H, Tan H, Tzempelikos A (2011). The effect of reflective coatings on building surface temperatures, indoor environment and energy consumption—An experimental study. *Energy and Buildings*, 43: 573–580.

Tian Z, Love JA (2008). A field study of occupant thermal comfort and thermal environments with radiant slab cooling. *Building and Environment*, 43: 1658–1670.

Trebilcock M, Soto-Muñoz J, Yañez M, Figueroa-San Martin R (2017). The right to comfort: A field study on adaptive thermal comfort in free-running primary schools in Chile. *Building and Environment,* 114: 455–469.

Welty JR (1978). Engineering Heat Transfer. New York: John Wiley & Sons.

Xamán J, Cisneros-Carreño J, Hernández-Pérez I, Hernández-López I, Aguilar-Castro KM, Macias-Melo EV (2017). Thermal Performance of a Hollow Block with/without Insulating and Reflective Materials for Roofing in Mexico. *Applied Thermal Engineering*, 123: 243–255.

Yuan J, Farnham C, Emura K (2015). Development of a retro-reflective material as building coating and evaluation on albedo of urban canyons and building heat loads. *Energy and Buildings*, 103: 107–117.

Zhou G, Pang M (2015a). Experimental investigations on thermal performance of phase change material–Trombe wall system enhanced by delta winglet vortex generators. *Energy*, 93: 758–769.

Zhou G, Pang M (2015b). Experimental investigations on the performance of a collector–storage wall system using phase change materials. *Energy Conversion and Management*, 105: 178–188.

Zhou Y, Zheng S, Chen H, Zhang G (2016). Thermal performance and optimized thickness of active shape-stabilized PCM boards for side-wall cooling and under-floor heating system. *Indoor and Built Environment*, 25: 1279–1295.

Zhou Y, Liu X, Zhang G (2017). Performance of buildings integrated with a photovoltaic-thermal collector and phase change materials. *Procedia Engineering*, 205: 1337–1343.

Zhu N, Liu P, Hu P, Liu F, Jiang Z (2015). Modeling and simulation on the performance of a novel double shape-stabilized phase change materials wallboard. *Energy and Buildings*, 107: 181–190.

Zhu N, Liu P, Liu F, Hu P, Wu M (2016). Energy performance of double shape-stabilized phase change materials wallboards in office building. *Applied Thermal Engineering*, 105: 180–188.